Research Article

Nano Biomed Eng

Silver Nanoparticles Synthesized by Cold Plasma as an Antibiofilm Agent against *Staphylococcus epidermidis* Isolated from Acne

Heba Khaleel Tawfeeq[1], Nisreen Kh. Abdalameer[2]✉, Rafal H. Jassim[2], Maryam M. Shehab[1]

[1] Department of Biology/ College of Science/ University of Baghdad, Baghdad, Iraq
[2] Department of Physics/ College of Science for Women/ University of Baghdad/ Baghdad, Iraq

✉ Corresponding author. E-mail: nisreenka_phys@csw.uobaghdad.edu.iq

Abstract

This study aimed to investigate the efficacy of silver nanoparticles (AgNPs) synthesized by cold plasma in inhibiting biofilm formed by *Staphylococcus epidermidis* both phenotypically and genotypically. The resultant AgNPs were characterized by using different parameters, color change, X-ray diffraction (XRD), zeta potential, feld emission scanning electron microscopy (FE-SEM), Fourier transform infrared (FTIR) spectroscopy, and transmission electron microscopy (TEM) methods. Moreover, their efficacy in inhibiting *S. epidermidis* biofilm was studied by the microtiter plate method. The results revealed that cold plasma succeeded in the synthesis of AgNPs with a size range of 10–20 nm. Markedly, the present findings indicated a significant decrease ($P < 005$) in the intensity of all tested biofilm alongside the down-regulation of accumulation-associated protein (*aap*) and *AtlE* in the presence of AgNPs as compared with non-treated cells. In conclusion, AgNPs synthesized by cold plasma acted as antibiofilm agents and could be used for pharmaceutical applications.

Keywords: silver nanoparticles (AgNPs); cold plasma; *Staphylococcus epidermidis*; biofilm

Introduction

The primary mode of growth for the microorganisms on the skin is through the formation of biofilms, which help to stabilize the resident microbial community and provide beneficial effects for both local and systemic host immunity [1]. Biofilms serve as a survival strategy by shielding the embedded cells from harsh environmental conditions, such as antimicrobials or immune-mediated clearance like phagocytosis [2]. Swolana, et al. [3] stated that the establishment of biofilm into three major steps:

adhesion, maturation, and dispersion (Fig. 1).
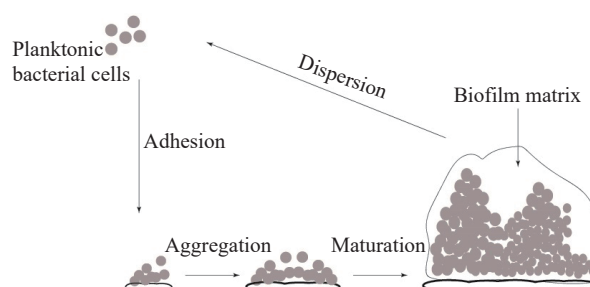
Fig. 1 Steps of biofilm formation in *Staphylococci* species.

The primary constituents of the staphylococcal biofilm matrix are polysaccharides, in particular,

polysaccharide intercellular adhesin (PIA), but can also include proteins like accumulation-associated protein (*aap*) and extracellular DNA [4]. According to Rohde, et al. [5], some strains of *Staphylococcus epidermidis* that are incapable of producing PIA can still create biofilms that rely on aap which has two domains (A and B) and is attached to the cell wall. Bacterial adhesion to epithelial cells and plastic surfaces is mediated by the A domain, while the B domain promotes cell–cell accumulation and biofilm formation when the A domain is broken down [6, 7]. Studies conducted on *S. epidermidis* is wild-type and an isogenic *AtlE* mutant showed that the majority of the extracellular DNA was generated by the autolysin *AtlE* in both *S. epidermidis* cultures and biofilms. According to the findings, extracellular DNA in *S. epidermidis* populations is produced when *AtlE* lyses a portion of the bacteria, and the extracellular DNA helps the remaining population build biofilms [8]. The biofilm produced by *S. epidermidis* exhibits a higher degree of antibiotic tolerance, and therefore, combination antibiotic therapy is necessary to effectively combat clinical isolates from infections related to catheters [9-11].

Scientists are actively searching for alternative compounds to counteract the growing resistance to antibiotics caused by the formation of biofilms. Among these compounds, silver nanoparticles (AgNPs) are widely recognized for their ability to combat bacterial cells. The effectiveness of AgNPs in inhibiting bacterial growth and preventing biofilm formation varies depending on factors such as their shape, concentration, and size.

Biomaterials in human medical care have included metal-based nanoparticles with anti-oxidant and antibacterial capabilities [12]. The distinctive biological, physical, and chemical characteristics exhibited by AgNPs in contrast to their larger-scale corresponding item have captured the attention and interest of numerous researchers and scholars [13]. AgNPs are widely used because of their potent antimicrobial action against both bacteria and fungi [14]. In light of the significant rise in biological and bacterial threats, particularly in sectors related to human consumption such as food, food packaging, and water, scientists are driven to create innovative inorganic nanoparticle substances with antibacterial properties. These substances are intended to be both user-friendly and devoid of any adverse side effects [15-17]. A discovery by scientists shows promise in

the battle against antibiotic resistance by using a laser to trigger the bactericidal activity of AgNPs. Due to its significant interaction with light, it might be developed as a medicine delivery method [18].

The present work aimed to test the impact of AgNPs prepared by plasma jets on *S. epidermidis* biofilm phenotypically and genotypically by investigating their effect on two biofilm-associated genes: *aap* and *AltE*.

Experimental

Synthesis of silver nitrite aqueous solution

For the preparation of 1 mmol/L aqueous solution, 0.008 493 5 g of $AgNO_3$ was dissolved in 50 mL of deionized water, thereafter, the solution was agitated gently to attain homogeneity.

Synthesis of AgNPs by microjet plasma technique

The generation of AgNPs requires the application of a high voltage, often in the range of 10 kV, This causes the aqueous solution of ($AgNO_3$) and the capillaries to become plasma. The assistance provided by the high-energy and ionically charged electrons (Ar) in the plasma results in a current of the order of a few milliampere-seconds (mA) flowing through the system. After the discharge has been turned on for a few minutes, the solutions will begin to take on a colour that may best be described as reddish-orange. It was thought that a duration of three minutes would be sufficient for each concentration. After that, an imprint was made in the coloured solution using a marking device. Afterwards, the device was removed.

A spectrophotometer with a wavelength range of 200–1 100 nm was used to learn more about the nanoparticles, the samples' UV–Visible (UV–Vis) absorption spectra were captured. Researchers used X-ray diffraction (XRD), zeta potential, Fourier transform infrared (FTIR) spectroscopy, field emission scanning electron microscopy (FE-SEM), and transmission electron microscopy (TEM) methods to characterize the synthetic AgNPs.

Estimation of minimal inhibitory concentration of AgNPs against *S. epidermidis*

The minimal inhibitory concentration (MIC) of AgNPs was determined by employing the broth

microdilution technique described by the Clinical and Laboratory Standards Institute [19]. Briefly, double serial concentrations of AgNPs (3.125, 6.25, 12.5, 25, 50, and 100 μg/mL) were prepared and placed in wells of flat bottom 96 well microtiter plates. Then, 10 μL of overnight diluted *S. epidermidis* suspension, adjusted to a 0.5 MacFarland turbidity standard, was added into all wells. Moreover, negative and positive controls were prepared as well.

Biofilm formation assay

S. epidermidis isolates were raised for 24 h at 37 °C in tryptic soy broth (TSB), then the inoculum concentration was adjusted to 1×10^8–2×10^8 CFU/mL using McFarland standard No. μL 0.5. This inoculum was divided into an aliquot of 200 μL, which was then put in three wells of a sterile 96-well microtiter plate and incubated for 24 h at 37 °C. After incubation, the liquid growth medium was carefully removed by inverting the plate and tapping it on a clean paper towel to remove any non-adherent cells. Thereafter, the wells were washed with sterile phosphate-buffered saline (PBS), to remove any remaining non-adherent cells and to prepare the biofilm for staining. A volume of 200 μL of methanol was applied into each well for 10 min and washed as previously mentioned. Afterwards, each well received 200 μL of 0.1% crystal violet, which was incubated there for 15 min at room temperature. The wash step was repeated three times. The plate was left for drying on a clean paper towel. Subsequently, For 10 min, 200 μL of 33% glacial acetic acid was added to each well. Finally, the absorbance of the stained biofilm was measured using a microplate reader at 600 nm. The amount of biofilm formed can be quantified by calculating the mean absorbance of the wells. The cut-off value (ODc) was calculated after the measurement of the biofilm-forming capacity for the study isolates alongside the negative controls. Nevertheless, ODc can be defined as triple standard deviations (SD) plus the negative control mean OD: for each microtiter plate, the ODc value was separately determined. It was presented as zero when a negative value was obtained, whereas the positive values indicated biofilm formation.

AgNPs effect on biofilm formation

A similar method addressed the biofilm formation was followed. However, tryptic soy broth containing AgNPs at ½MIC of each isolate was used. All plates were cultivated for a duration of 24 h at a temperature of 37 ºC. Following the completion of well washing, staining, and subsequent reading at 600 nm, positive controls were also conducted. This required the addition of 200 μL of a brand-new, 0.5 McFarland standard-compatible bacterial culture devoid of AgNPs.

Gene expression of *aap* and *AtlE* genes by RT-qPCR

The gene expression of *aap* and *AtlE* genes was measured before and after treatment with the AgNPs (at ½MIC) for each isolate, as follows:

RNA Extraction

The RNA was extracted with TRIzol™ reagent (Invitrogen, USA) according to the manufacturer's instructions and the concentration and purity were measured using the Qubit 4 (ThermoFisher®, USA). cDNA was synthesized using ProtoScript® First Strand cDNA Synthesis Kit(NEB, UK). The resultant cDNA was quantified by using Qubit™ dsDNA H.S. Assay Kit (ThermoFisher®, USA).

Quantitative RT-qPCR

Quantitative detection was based on Syber Green's fluorescence power. The reaction mixture was composed of the following components, with their quantities as shown in Table 1. After that, the real-time PCR program was set up using the specified thermocycling protocol as shown in Table 2.

Table 1 RT-qPCR component

Reacatant	Volume (μL)
Luna Universal qPCR Master Mix	10
Forward primer (10 μmol/L)	1
Reverse primer (10 μmol/L)	1
Template cDNA (ng/μL)	5
Nuclease-free water	3

Table 2 Thermocycling protocol and conditions

Step	Temperature (°C)	Time	Number of cycles
Initial denaturation	95	60 s	1
Denaturation	95	15 s	45
Extension	60	30 s	
Melt curve	60–95	40 min	1

The analysis of gene expression follows the Livak formula. Following the normalization of these results

to the rpoB gene's expression, the following results were obtained:

$$\text{Fold change} = 2^{-\Delta\Delta Ct} \tag{1}$$

$$\Delta\Delta Ct = \Delta Ct(\text{Treatment})\Delta Ct(\text{Control}) \tag{2}$$

$$\Delta Ct = Ct \text{ of target gene} - Ct \text{ of a housekeeping gene} \tag{3}$$

Results

UV–Vis spectroscopy

It is one of the methods that is used the most often in the process of identifying a broad variety of substances, including ions of transition metals, chemical compounds, and biological molecules. The colour of the silver colloidal solutions goes from being colourless to a yellowish colour, which is the first proof that a synthesis process has occurred. The first step in the process of characterizing AgNPs and their oxides consisted of doing a UV–Vis examination. It was noted that the highest absorption occurred at 404 nm, which is where the maximum absorption represents the surface plasmon resonance of AgNPs (Fig. 2). In the context of UV–Vis spectroscopy analysis of silver (Ag) nanoparticles, the presence of a distinct peak preceding the 400 nm wavelength range can be ascribed to the occurrence of surface plasmon resonance (SPR) phenomena. When examining Ag nanoparticles, it is commonly observed that the hump generally leads to a change toward shorter wavelengths, known as a blue shift, rather than a shift toward longer wavelengths, known as a redshift. As a result of the phenomenon known as SPR: The optical characteristics of silver nanoparticles are characterized by the collective oscillation of their conduction electrons in response to input electromagnetic radiation, notably within the UV–Vis range. The term used to describe this occurrence is surface plasmon resonance. Strong absorption of light happens when the frequency (or energy) of incident photons aligns with the natural frequency of electron oscillations. The phenomenon of a blue shift is frequently observed in the context of SPR in silver nanoparticles. A blue shift refers to the phenomenon when the absorption peak of a material shifts towards shorter wavelengths, indicating higher energy levels, in comparison to the anticipated wavelength for silver in its bulk form. The phenomenon of blue shift arises due to the impact of nanoparticle size and shape on the wavelength of

SPR. The energy SPR peaks of smaller nanoparticles exhibit greater values, resulting in a phenomenon known as a blue shift in comparison to bulk silver. As the dimensions of nanoparticles shrink, the phenomenon of collective electron oscillations takes place at higher frequencies, which are associated with shorter wavelengths. The morphology of nanoparticles can potentially exert an influence on the wavelength of SPR. As an illustration, it has been observed that spherical nanoparticles exhibit a somewhat distinct SPR wavelength in comparison to alternative geometries, such as nanorods or nanostars.
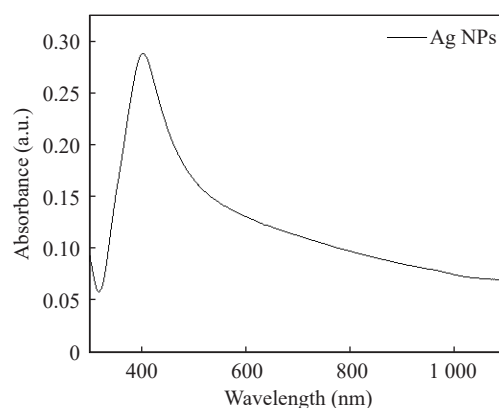
Fig. 2 UV–Vis spectrum absorption of AgNPs prepared by cold plasma in the range of 300–1 100 nm

XRD analysis

Through the use of X-ray diffraction pattern analysis, it was discovered that the sample of AgNPs that had been exposed to the standard conditions possessed a crystalline structure. Crystallographic structure, preferred orientation, and grain size were all characterized by this method. XRD examination performed on Ag nanoparticles revealed a series of Bragg reflection peaks at 2θ of 38.31°, 44.49°, 64.61°, and 77.53°, as shown in Fig. 3. These figures represent, successively, the crystal facets of the (111),
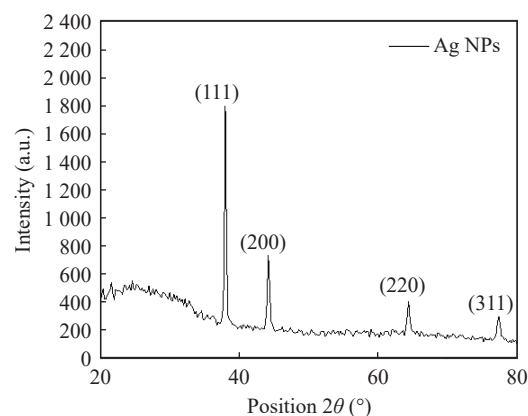
Fig. 3 XRD pattern of AgNPs prepared by cold plasma

(200), (220), and (311) planes of the face-centred cubic structure of silver.

Following the conventional diffraction pattern of JCPDS No. 89-3722, the findings of the XRD experiment demonstrated unequivocally that the AgNPs that were produced by the reduction of Ag^+ ions have a crystalline structure. Using the Debye-Scherrer equation [20], one can determine the typical particle size of the AgNPs that were produced by the cold plasma method:

$$D = k\lambda / (\beta\cos\theta) \tag{4}$$

where β is the Full-Width at Half-Maximum measured in radians, k is the crystallite shape factor a good approximation is 0.9, λ is X-ray wavelength, and θ is Bragg's angel. It was found that the average size was approximately 12 nm for AgNPs (Table 3).

Table 3 The structural and geometric parameters of AgNPs

Nanoparticles	Position (°)	d-spacing (A°)	FWHM (β)	(hkl)	Crystalline size (nm)
	38.31	2.01	0.476	111	17.58
	44.49	1.89	0.536	200	15.12
Ag	64.61	1.35	0.557	220	14.54
	77.53	1.19	0.61	311	12.44

Zeta Potential of AgNPs

The stability of the AgNPs was performed by using zeta potential analysis. Zeta potential values reveal information regarding the surface charge and stability of the synthesized AgNPs. Figure 4 depicted the zeta potential value of the colloidal solution of AgNPs to be −11.60 mV which is indicative of their small size and high stability.
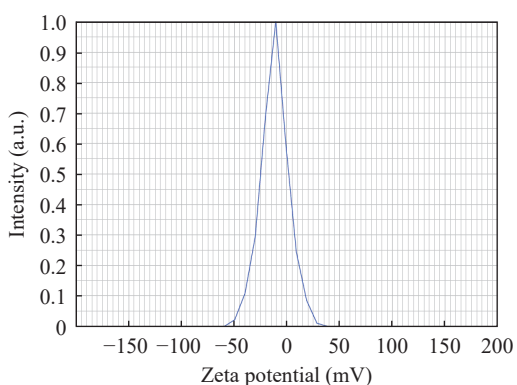
Fig. 4 Graph result for Zeta potential of AgNPs prepared by cold plasma.

FE-SEM analysis of AgNPs

By using FE-SEM analysis, one can gather information such as the grain size and shape. The surface morphology of the cold plasma-synthesized AgNPs with 0.01 molarity concentrations of silver nitrate obtained is indicated in the FE-SEM image depicted in Fig. 5. The FE-SEM images of the AgNPs demonstrate their granular nano-sized range and uniform distribution, characterized by spherical-shaped particles that are agglomerated.
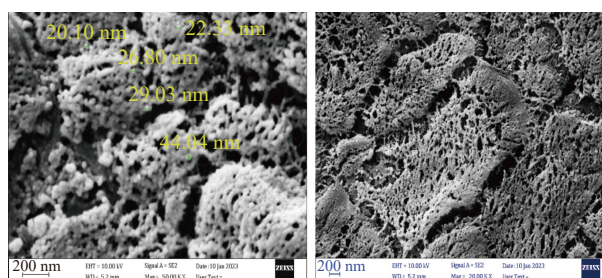
Fig. 5 FE- SEM image of AgNPs prepared by cold plasma with nanoscale 200 nm

TEM analysis of AgNPs

To analyze the size, shape, and morphology of the AgNPs synthesized through cold plasma, TEM was utilized. The obtained image, as depicted in Fig. 6, clearly indicated that the particle size of AgNPs ranged from 10 to 20 nm. The presence of larger AgNPs could potentially be attributed to the aggregation of the smaller nanoparticles, which may have occurred during the TEM measurements. These results proved that the particles have a spherical shape and non-uniform distribution (monodispersed) without any important agglomeration.
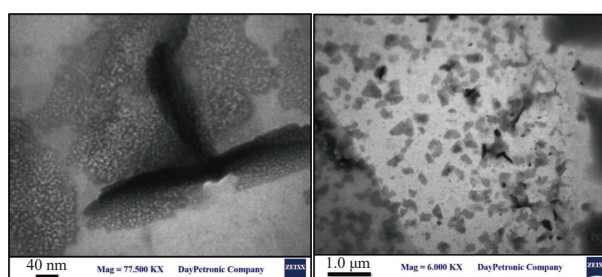
Fig. 6 Transmission electron micrograph of AgNPs prepared by cold plasma with nanoscale 40 nm and 1.0 μm

FTIR analysis of AgNPs

The chemical changes in functional groups within a composite can be revealed through the analysis of FTIR absorption spectra. Figure 6 depicts the FTIR analysis of the obtained AgNPs, which proves to be a useful method for characterizing the surface chemistry of nanoparticles. The FTIR spectra displayed in both figures exhibit absorption peaks

corresponding to stretching vibrations of hydroxyl (O-H) groups, alkane (C-H) groups, aliphatic amines (C-O) groups, and carboxylic acid (C=O) groups, indicating their presence in the synthesis process of the nanoparticles as shown in Fig. 7. Additionally, in both figures, the band below 600 cm^{-1} can be attributed to the formation of AgNPs and their oxides.
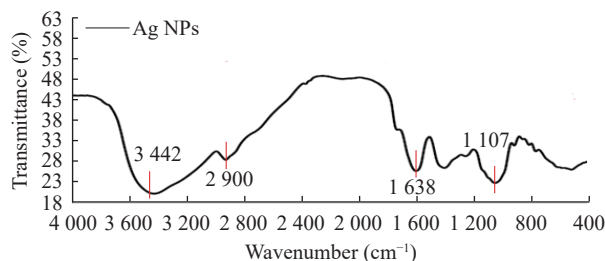
Fig. 7 FTIR absorption spectra of AgNPs prepared by cold plasma.

AgNPs MIC

The results grouped in Table 4 summarized the MIC of AgNPs.

Table 4 MIC of AgNPs against Staphylococcus epidermidis

Isolate No.	MIC (μg/mL)
SE1	50
SE2	25
SE3	50
SE4	25
SE5	25
SE6	12.5
SE7	25
SE8	12.5
SE9	50
SE10	12.5
SE11	25
SE12	50
SE13	25
SE14	12.5
SE15	50

Effect of AgNPs on Biofilm

The AgNPs significantly reduced the biofilm intensity as highlighted in Fig. 8 and Table 5.

Gene expression

Data highlighted in Fig. 9 indicated that AgNPs inhibited the gene expression of *aap* and *AtlE*
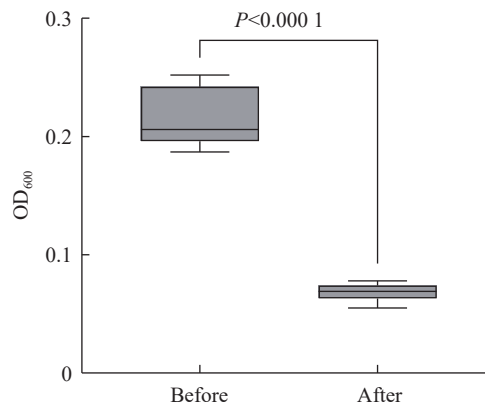
Fig. 8 Box plot of biofilm *S. epidermidis* affected by AgNPs.

Table 5 Influence of AgNPs on biofilm produced by *S. epidermidis* isolates

Isolate code	OD$_{600}$ ± SD		P-value
	Before treatment	After treatment	
SE1	0.196 ± 0.06	0.069 ± 0.05	1.2×10^{-5}
SE2	0.187 ± 0.041	0.078 ± 0.043	5.2×10^{-5}
SE3	0.225 ± 0.013	0.075 ± 0.05	0.000 8
SE4	0.206 ± 0.05	0.074 ± 0.021	0.000 6
SE5	0.193 ± 0.03	0.064 ± 0.04	3.3×10^{-6}
SE6	0.23 ± 0.026	0.073 ± 0.03	0.008
SE7	0.25 ± 0.053	0.069 ± 0.097	0.021
SE8	0.198 ± 0.07	0.058 ± 0.08	2.8×10^{-5}
SE9	0.218 ± 0.08	0.063 ± 0.03	0.000 2
SE10	0.196 ± 0.06	0.068 ± 0.054	0.000 7
SE11	0.199 ± 0.09	0.056 ± 0.06	6.3×10^{-5}
SE12	0.244 ± 0.04	0.055 ± 0.051	1.4×10^{-6}
SE13	0.252 ± 0.02	0.075 ± 0.055	3.9×10^{-5}
SE14	0.201 ± 0.01	0.063 ± 0.03	3.5×10^{-5}
SE15	0.22 ± 0.02	0.069 ± 0.09	0.001
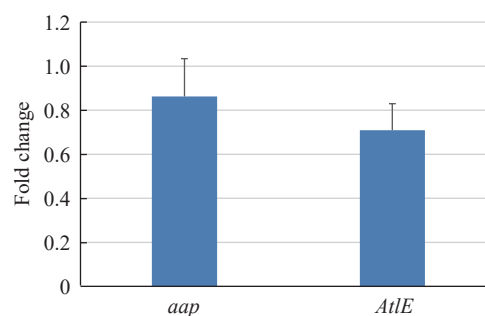
Fig. 9 Effect of AgNPs on the gene expression of *aap* and *AtlE*. Error bars represent standard deviation.

Discussion

The characteristic absorption band of AgNPs typically falls within the range of 350–450 nm. The

asymmetrical and narrow SPR band suggests that the AgNPs possess a uniform shape and a narrow size distribution [21-23]. Upon these facts and regarding the results illustrated in Fig. 2, It was noted that the highest absorption occurred at 404 nm, which confirms that the synthesized particles are AgNPs.

Numerous studies have documented the antibiofilm activity of AgNPs towards human pathogens such as *Klebsiella pneumoniae, Escherichia coli* [24], and *S. aureus* emphasizing their possibility as surrogate antibiofilm [25]. The activity of nanoparticles, such as AgNPs, is influenced by their size and shape, as smaller sizes result in a larger surface contact area between AgNPs and microorganisms [26]. The present work used spherical AgNPs with a diameter of 10–20 nm (Figs. 4 and 6). Parallel earlier investigations were carried out and reached various sizes, of which, Salman, et al. [25] synthesized AgNPs with a diameter of 20–100 nm using pulsed laser ablation in liquid. Saleh and Najim [27] produced AgNPs of different sizes ranging from 74–77 nm using plant extract as a reducing agent. Recalling the findings depicted in Fig. 4, the stability of the AgNPs could potentially be attributed to the intricate composition of the aqueous extracts, which may have acted as protective coating agents. In contrast to other documented methods for synthesizing AgNPs, the current preparations did not necessitate any supplementary steps for the coating to ensure the stability of AgNPs and avert their aggregation.

There have been reports that AgNPs may prevent bacteria from forming biofilms either by interacting with the biofilm's core ingredients or by causing structural damage to the biofilm itself [28]. The activity of nanoparticles on microbial cells and the biofilms they produce may be broken down into two primary categories. To begin, it causes direct damage to the cytoplasmic membrane as well as the components of the cell. Second, the creation of reactive oxygen species (ROS) may induce increasing bacterial membrane permeability and inactivation of proteins, RNA, and DNA that are already present in the cells [29]. Moreover, AgNPs may prevent biofilm formation by quenching bacterial quorum sensing, thus blocking signals for biofilm formation [30].

The survival of bacterial cells is significantly compromised by bactericidal activity, which is attributed to the release of silver ions from nanoparticles [31]. The mechanism by which they act against *Staphylococci* involves causing irreparable damage to bacterial cells through various means, including inhibition of bacterial DNA replication, degradation of bacterial cytoplasmic membranes, and modification of intracellular adenosine-5′-triphosphate (ATP) levels [32]. Silver ions have a great attraction for electron-donating groups including sulfhydryl, carbonyl, and phosphate groups, which are frequently present in proteins or cell membranes. They can also bind to the thiol groups of proteins, changing their three-dimensional structure and obstructing the active binding sites in the process [31]. Due to their unique structure and multiple modes of interaction with bacterial cell membranes, they possess a distinctive ability to counteract bacterial growth [33].

Nevertheless, The present investigation suggested that AgNPs inhibited biofilm formation in *S. epidermidis* (Fig. 8 and Table 5) via down-regulation of biofilm-associated genes; *aap* and *atlE*. To the best of our knowledge, this is the first report to document the effect of ANPs on *aap* and *AtlE* genes of *S. epidermidis*; hence, we could not find any investigations to compare our results with it.

The non-thermal atmospheric pressure plasma sources that produce a wide array of reactive oxygen and nitrogen species (RONS) are essential to the success of this application [34]. Because RONS created by plasma may alter the chemical makeup of a liquid, plasma-liquid interactions are a key step in the production of nanomaterials. The principal forms of reactive oxygen and nitrogen species (RONS) that are produced as a result of interactions between plasma and liquid are hydroxyl radical, hydrogen peroxide, superoxide, ozone, singlet oxygen, nitric oxide, and others [35].

The toxicity of AgNPs is influenced by various factors, including concentration, shape, surface properties, and size [36]. Within the field of dermatology, AgNPs have been found to induce cytotoxicity in keratinocytes *in vitro*, and they are observed to be deposited either in or on the stratum corneum in vivo [37]. However, it is worth noting that no acute dermal toxicity was observed at high concentrations [38]. In comparison to earlier investigations, which assessed the toxicity of nanospheres ranging from 10 to 20 nm, the concentration utilized in the current investigation was

relatively low.

Conclusions

AgNPs prepared by cold plasm technique reduced the intensity of all tested biofilms; which was accompanied by the downregulation of *aap* and *AtlE*. Upon that, the current study proposed that the inhibition of biofilm formation in *S. epidermidis* was caused by AgNPs through the suppression of genes linked to biofilm formation, namely *aap* and *AtlE*.

CRediT Author Statement

Heba Khaleel Tawfeeq: data curation, writing–review, and editing. **Nisreen Kh. Abdalameer**: conceptualization, investigation, and methodology. **Rafal H. Jassim**: project administration and supervision. **Maryam M. Shehab:** visualization and writing – original.

Acknowledgement

Conflict of Interests

All authors declare that there is no conflict of interest.

References

[1] R.L. Gallo. Human skin is the largest epithelial surface for interaction with microbes. *Journal of Investigative Dermatology*, 2017, 137(6): 1213−1214. https://doi.org/10.1016/j.jid.2016.11.045

[2] Di Domenico, E., I. Farulla, G. Prignano, et al. Biofilm is a major virulence determinant in bacterial colonization of chronic skin ulcers independently from the multidrug resistant phenotype. *International Journal of Molecular Sciences*, 2017, 18(5): 1077. https://doi.org/10.3390/ijms18051077

[3] D. Swolana, M. Kępa, C. Kruszniewska-Rajs, et al. Antibiofilm effect of silver nanoparticles in changing the biofilm-related gene expression of staphylococcus epidermidis. *International Journal of Molecular Sciences*, 2022, 23(16): 9257. https://doi.org/10.3390/ijms23169257

[4] M. Loza Correa, J. Ayala, I. Perelman, et al. Biofilm matrix and cell wall modification during biofilm formation might confer *Staphylococcus epidermidis* advantageous growth in platelets. Abstract 4C-S28-02. *Vox Sang*, 2017, 112(Suppl. 1): 63–64

[5] H. Rohde, C. Burdelski, K. Bartscht, et al. Induction of *Staphylococcus epidermidis* biofilm formation via proteolytic processing of the accumulation-associated protein by staphylococcal and host proteases. *Molecular Microbiology*, 2005, 55(6): 1883−1895. https://doi.org/10.1111/j.1365-2958.2005.04515.x

[6] A.E. Paharik, M. Kotasinska, A. Both, et al. The metalloprotease SepA governs processing of accumulation-associated protein and shapes intercellular adhesive surface properties in *Staphylococcus epidermidis*. *Molecular Microbiology*, 2017, 103(5): 860–874. https://doi.org/10.1111/mmi.13594

[7] A.E. Yarawsky, S.L. Johns, P. Schuck, et al. The biofilm adhesion protein Aap from *Staphylococcus epidermidis* forms zinc-dependent amyloid fibers. *Journal of Biological Chemistry*, 2020, 295(14): 4411−4427. https://doi.org/10.1074/jbc.RA119.010874

[8] A. Marek, E. Pyzik, D. Stępień-Pyśniak, et al. Biofilm-formation ability and the presence of adhesion genes in coagulase-negative staphylococci isolates from chicken broilers. *Animals*, 2021, 11(3): 728. https://doi.org/10.3390/ani11030728

[9] M. Fournière, T. Latire, D. Souak, et al. *Staphylococcus epidermidis* and cutibacterium acnes: Two major sentinels of skin microbiota and the influence of cosmetics. *Microorganisms*, 2020, 8(11): 1752. https://doi.org/10.3390/microorganisms8111752

[10] J.A. Koch, T.M. Pust, A.J. Cappellini, et al. *Staphylococcus epidermidis* biofilms have a high tolerance to antibiotics in periprosthetic joint infection. *Life*, 2020, 10(11): 253. https://doi.org/10.3390/life10110253

[11] K.E. Daffinee, E.C. Piehl, C. Bleick, et al. Eradication of *Staphylococcus epidermidis* within biofilms: Comparison of systemic versus supratherapeutic concentrations of antibiotics. *Antimicrobial Agents and Chemotherapy*, 2023, 67(6): e0010823. https://doi.org/10.1128/aac.00108-23

[12] T. Rasheed, M. Bilal, H.M.N. Iqbal, et al. Green biosynthesis of silver nanoparticles using leaves extract of *Artemisia vulgaris* and their potential biomedical applications. *Colloids and Surfaces B*: *Biointerfaces*, 2017, 158: 408−415. https://doi.org/10.1016/j.colsurfb.2017.07.020

[13] R.L. Wang, Y.Q. Shang, P. Kanjanaboos, et al. Colloidal quantum dot ligand engineering for high performance solar cells. *Energy & Environmental Science*, 2016, 9(4): 1130−1143. https://doi.org/10.1039/c5ee03887a

[14] M.M.A. Al-Mousawi, A. Al-Nafiey, G. Al-Dahesh. Studying the effect of the number of laser pulses on the structure, morphology, and optical properties for a thin film of GO-Ag nanocomposites. *Journal of Physics*: *Conference Series*, 2021, 1999(1): 012141. https://doi.org/10.1088/1742-6596/1999/1/012141

[15] S. Khorrami, A. Zarrabi, M. Khaleghi, et al. Selective cytotoxicity of green synthesized silver nanoparticles against the MCF-7 tumor cell line and their enhanced antioxidant and antimicrobial properties. *International Journal of Nanomedicine*, 2018, 13: 8013−8024. https://doi.org/10.2147/ijn.s189295

[16] M.J.M. Al-Shaabani, A.M.T. Al-Ethawi, H.J.F. Al-Mathkhury. Eco-frienly synthesis of gold nanoparticles and study their effect with antibiotics against acinetobacter baumannii. *Iraqi Journal of Agricultural Sciences*, 2020, 51(4): 1204−1211. https://doi.org/10.36103/ijas.v51i4.1099

[17] M.J.M. Al-Shaabani, A.M. Turki, H.J.F. Al-Mathkhury. The antibiofilm efficacy of gold nanoparticles against acinetobacter baumannii. *Iraqi Journal of Science*, 2020: 749–753. https://doi.org/10.24996/ijs.2020.61.4.6

[18] L.L. Lin, S.A. Starostin, S.R. Li, et al. synthesis of metallic nanoparticles by microplasma. In: Metallic Nanomaterials (Part A). De Gruyter, 2018: 49–102. https://doi.org/10.1515/9783110345100-002

[19] Performance Standards for Antimicrobial Susceptibility Testing, M100, 33rd ed. Clinical and Laboratory Standards Institute, 2023.

[20] M. Rabiei, A. Palevicius, A. Monshi, et al. Comparing methods for calculating nano crystal size of natural hydroxyapatite using X-ray diffraction. *Nanomaterials*, 2020, 10(9): 1627. https://doi.org/10.3390/nano10091627

[21] S. Yallappa, J. Manjanna, S.K. Peethambar, et al. Green synthesis of silver nanoparticles using acacia farnesiana (sweet acacia) seed extract under microwave irradiation and their biological assessment. *Journal of Cluster Science*, 2013, 24(4): 1081−1092. https://doi.org/10.1007/s10876-013-0599-7

[22] O. Velgosová, A. Mražíková, R. Marcinčáková. Influence of pH on green synthesis of Ag nanoparticles. *Materials Letters*, 2016, 180: 336−339. https://doi.org/10.1016/j.matlet.2016.04.045

[23] E. Mossé Alhadeff, A. Jackson Telles Bosco, C. Fragale Pastusiak, et al. Development of an ethanol biosensor based on silver nanoparticles/polyaniline/graphite/epoxy composite for friendly analytical application. In: Biosensors for Environmental Monitoring. T. Rinken, K. Kivirand, Eds. IntechOpen, 2019. https://doi.org/10.5772/intechopen.89359

[24] S.O. Hasson, S.A.K. Salman, S.F. Hassan, et al. Antimicrobial effect of eco- friendly silver nanoparticles synthesis by Iraqi date palm (Phoenix dactylifera) on gram-negative biofilm-forming bacteria. *Baghdad Science Journal*, 2021, 18(4): 1149. https://doi.org/10.21123/bsj.2021.18.4.1149

[25] O. N. Salman, M. O. Dawood, D. S. Ahmed. Antibacterial activity of gold and silver nanoparticles against pathogen species, *E. coli* and *S. aureus*. *Iraqi Journal of Applied Physics,* 2017, 13(3).

[26] M. Seo, T. Oh, S. Bae. Antibiofilm activity of silver nanoparticles against biofilm forming Staphylococcus pseudintermedius isolated from dogs with otitis externa. *Veterinary Medicine and Science*, 2021, 7(5): 1551−1557. https://doi.org/10.1002/vms3.554

[27] G.M. Saleh, S.S. Najim. Antibacterial activity of silver nanoparticles synthesized from plant latex. *Iraqi Journal of Science*, 2020: 1579–1588. https://doi.org/10.24996/ijs.2020.61.7.5

[28] A.A. Ashkarran. A novel method for synthesis of colloidal silver nanoparticles by arc discharge in liquid. *Current Applied Physics*, 2010, 10(6): 1442−1447. https://doi.org/10.1016/j.cap.2010.05.010

[29] M. Govarthanan, S. Thangasamy, M. Koildhasan, et al. Biosynthesis and characterization of silver nanoparticles using panchakavya, an Indian traditional farming formulating agent. *International Journal of Nanomedicine*, 2014, 9(1): 1593−1599. https://doi.org/10.2147/ijn.s58932

[30] P.R. Chaudhari, S.A. Masurkar, V.B. Shidore, et al. Effect of biosynthesized silver nanoparticles on staphylococcus aureus biofilm quenching and prevention of biofilm formation. *Nano-Micro Letters*, 2012, 4(1): 34−39. https://doi.org/10.1007/BF03353689

[31] D.Y. Leng, Y. Li, J. Zhu, et al. The antibiofilm activity and mechanism of nanosilver- and nanozinc-incorporated mesoporous calcium-silicate nanoparticles. *International Journal of Nanomedicine*, 2020, 15: 3921−3936. https://doi.org/10.2147/ijn.s244686

[32] G. Franci, A. Falanga, S. Galdiero, et al. Silver nanoparticles as potential antibacterial agents. *Molecules*, 2015, 20(5): 8856−8874. https://doi.org/10.3390/molecules20058856

[33] H.X. Ji, S.N. Zhou, Y.Q. Fu, et al. Size-controllable preparation and antibacterial mechanism of thermo-responsive copolymer-stabilized silver nanoparticles with high antimicrobial activity. *Materials Science and Engineering: C*, 2020, 110: 110735. https://doi.org/10.1016/j.msec.2020.110735

[34] T. Huang, S. Kumari, H. Herold, et al. Enhanced antibacterial activity of Se nanoparticles upon coating with recombinant spider silk protein eADF$_4$(κ16). *International Journal of Nanomedicine*, 2020, 15: 4275−4288. https://doi.org/10.2147/ijn.s255833

[35] P.S. Vankar, D. Shukla. Biosynthesis of silver nanoparticles using lemon leaves extract and its application for antimicrobial finish on fabric. *Applied Nanoscience*, 2012, 2(2): 163−168. https://doi.org/10.1007/s13204-011-0051-y

[36] C.A. Dos Santos, M.M. Secker, A.P. Ingle, et al. Silver nanoparticles: Therapeutical uses, toxicity, and safety issues. *Journal of Pharmaceutical Sciences*, 2014, 103(7): 1931−1944. https://doi.org/10.1002/jps.24001

[37] M.E. Samberg, S.J. Oldenburg, N.A. Monteiro-Riviere. Evaluation of silver nanoparticle toxicity in skin *in vivo* and keratinocytes *in vitro*. *Environmental Health Perspectives*, 2010, 118(3): 407–413. https://doi.org/10.1289/ehp.0901398

[38] S. Kim, D.-Y. Ryu. Silver nanoparticle‐induced oxidative stress, genotoxicity and apoptosis in cultured cells and animal tissues. *Journal of applied toxicology*, 2013, 33(2): 78−89. https://doi.org/10.1002/jat.2792